Attention Guided Anomaly Detection and Localization in Images

Shashanka Venkataramanan[*1], Kuan-Chuan Peng[†1], Rajat Vikram Singh[‡], and Abhijit Mahalanobis[*]

[*]Center for Research in Computer Vision, University of Central Florida, Orlando, FL
[†]Mitsubishi Electric Research Laboratories, Cambridge, MA
[‡]Siemens Corporate Technology, Princeton, NJ

shashankv@Knights.ucf.edu, kpeng@merl.com, singh.rajat@siemens.com, amahalan@crcv.ucf.edu

Abstract

Anomaly detection and localization is a popular computer vision problem involving detecting anomalous images and localizing anomalies within them. However, this task is challenging due to the small sample size and pixel coverage of the anomaly in real-world scenarios. Prior works need to use anomalous training images to compute a threshold to detect and localize anomalies. To remove this need, we propose Convolutional Adversarial Variational autoencoder with Guided Attention (CAVGA), which localizes the anomaly with a convolutional latent variable to preserve the spatial information. In the unsupervised setting, we propose an attention expansion loss, where we encourage CAVGA to focus on all normal regions in the image without using any anomalous training image. Furthermore, using only 2% anomalous images in the weakly supervised setting we propose a complementary guided attention loss, where we encourage the normal attention to focus on all normal regions while minimizing the regions covered by the anomalous attention in the normal image. CAVGA outperforms the state-of-the-art (SOTA) anomaly detection methods on the MNIST, CIFAR-10, Fashion-MNIST, MVTec Anomaly Detection (MVTAD), and modified ShanghaiTech Campus (mSTC) datasets. CAVGA also outperforms the SOTA anomaly localization methods on the MVTAD and mSTC datasets.

1. Introduction

With several breakthroughs of Deep Neural Networks (DNNs) outperforming humans in the field of image classification [13], action recognition [10], face recognition [23], etc., one area where it has made significant progress is recognizing whether an image is homogeneous with its

---

[1]This work was done when Shashanka Venkataramanan was an intern and Kuan-Chuan Peng was a staff scientist at Siemens Corporate Technology.
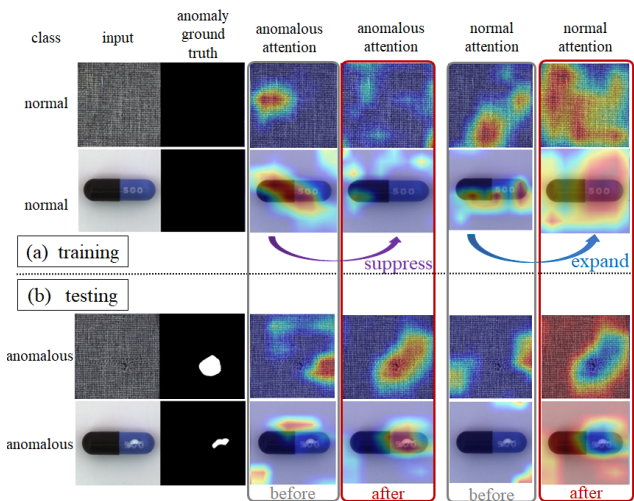

Figure 1. CAVGA uses the proposed complementary guided attention loss to encourage a normal attention that expands to the entire image of the normal training image while suppressing its anomalous attention, which enables the trained network to generate the anomalous attention map better localizing the anomaly at testing.

previously observed distribution or whether it belongs to a novel or anomalous distribution [1]. To develop machine learning algorithms for such a setting can be challenging due to the lack of suitable data since images with anomalies are rarely available in real world scenarios as discussed by [3]. Prior works on anomaly detection employ handcrafted features to detect anomalies [2, 5, 35], while [9, 12] propose autoencoder based networks in such challenging settings. GAN based approaches [31, 41] have also been proposed for this task. [36, 38] propose temporal anomaly localization while [7] proposes patch based anomaly localization in videos. Trained with normal images or videos, these methods use a thresholded pixel-wise difference between the input and reconstructed image to detect and localize anomalies. However, their methods need to use anomalous training images to determine the threshold which can be unavailable in real-world scenarios.

To remove this need, we propose Convolutional Adversarial Variational autoencoder with Guided Attention (CAVGA), an unsupervised anomaly detection and localization method which requires no anomalous training images. In case when few anomalous training images are available, we also extend CAVGA to a weakly supervised setting. Without any prior knowledge of the anomaly, in general, it is required to look at the entire image to localize the anomaly, based on which we design the guided attention mechanism in CAVGA. In the unsupervised setting comprising of only normal images during training [3], we encourage the network to focus on all normal regions of the image such that the feature representation of the latent variable encodes all the normal regions. In the weakly supervised setting, we introduce a classifier in CAVGA and propose a complementary guided attention loss computed only for the normal images correctly predicted by the classifier. Using this complementary guided attention loss, we expand the normal images' normal attention but suppress their anomalous attention, where normal/anomalous attention represents the areas affecting the classifier's normal/anomalous prediction identified by existing network visualization methods (e.g. Grad-CAM [34]). Figure 1 (a) illustrates our guided attention mechanism, and we find that it improves the performance of anomaly localization (shown in Sec. 5), and the resulting normal attention and anomalous attention of anomalous testing images are visually complementary, which is consistent with our intuition, as illustrated in Figure 1 (b).

To the best of our knowledge, we are the first in anomaly detection and localization to propose an end-to-end trainable framework with attention guidance which explicitly enforces the network to learn representations from the entire normal images. As compared to the prior works, our proposed approach CAVGA needs no anomalous training images to determine a threshold to detect and localize the anomaly. Our contributions are:

- **Convolutional adversarial variational autoencoder with guided attention (CAVGA)**, which comprises of a convolutional latent variable to preserve the spatial relation between the input and latent variable as compared to flattening it.

- **An attention expansion loss (L_{ae})**, where we encourage the network to focus on the entire normal images in the unsupervised setting.

- **A complementary guided attention loss (L_{cga})**, using which we minimize the anomalous attention and simultaneously expand the normal attention for the normal images correctly predicted by the classifier.

- **New SOTA**: In anomaly detection, CAVGA outperforms the SOTA methods on the MVTAD [3], mSTC [22], MNIST [19], CIFAR-10 [17] and Fashion-MNIST [39] datasets in classification accuracy. In anomaly localization, CAVGA outperforms the SOTA methods on the mSTC datasets in IoU and mean Area under ROC curve (AuROC). CAVGA also outperforms the SOTA anomaly localization methods on the MVTAD dataset in IoU, and performs on par with the SOTA anomaly localization methods in AuROC.

2. Proposed approach: CAVGA

2.1. Unsupervised approach: CAVGA$_u$

Figure 2 (a) illustrates CAVGA in the unsupervised setting (denoted as CAVGA$_u$). CAVGA$_u$ comprises of a convolutional latent variable as compared to flattened one, to preserve the spatial information between the input and latent variable. Since attention maps obtained from feature maps illustrate the regions of the image responsible for specific activation of neurons in it [40], we propose an attention expansion loss such that the feature representation of the latent variable encodes all the normal regions. This loss encourages the attention map generated from the latent variable to cover the entire normal training image as illustrated in Figure 1 (a). During testing, we localize the anomaly from the anomalous attention map of the input image.

2.1.1 Convolutional latent variable

Variational Autoencoder (VAE) [15] is a generative model widely used for anomaly detection [16, 29]. The loss function of training a vanilla VAE can be formulated as:

$$L = L_R(x, \hat{x}) + KL(q_\phi(z|x)||p_\theta(z|x)), \quad (1)$$

where $L_R(x, \hat{x}) = \frac{-1}{N} \sum_{i=1}^{N} x_i log(\hat{x}_i) + (1 - x_i)log(1 - \hat{x}_i)$, x is the input image, $\hat{x}$ is the reconstructed image, and N is the total number of images. The posterior $p_\theta(z|x)$ is modeled using a standard Gaussian distribution prior $p(z)$ with the help of Kullback-Liebler (KL) divergence through $q_\phi(z|x)$. Since the vanilla VAE results in blurry reconstruction [18], we use a discriminator ($D(.)$) to improve the stability of the training and generate a sharper reconstruction $\hat{x}$ using adversarial learning [25] formulated as follows:

$$L_{adv} = -\frac{1}{N} \sum_{i=1}^{N} log(D(x_i)) + log(1 - D(\hat{x}_i)) \quad (2)$$

Unlike traditional autoencoders [4, 11] where the latent variable is vectorized, inspired from [26], we propose to use a convolutional latent variable to preserve the spatial relation between the input and the latent variable. We illustrate the effectiveness of using a convolutional latent variable over vectorizing it in Sec. 5.
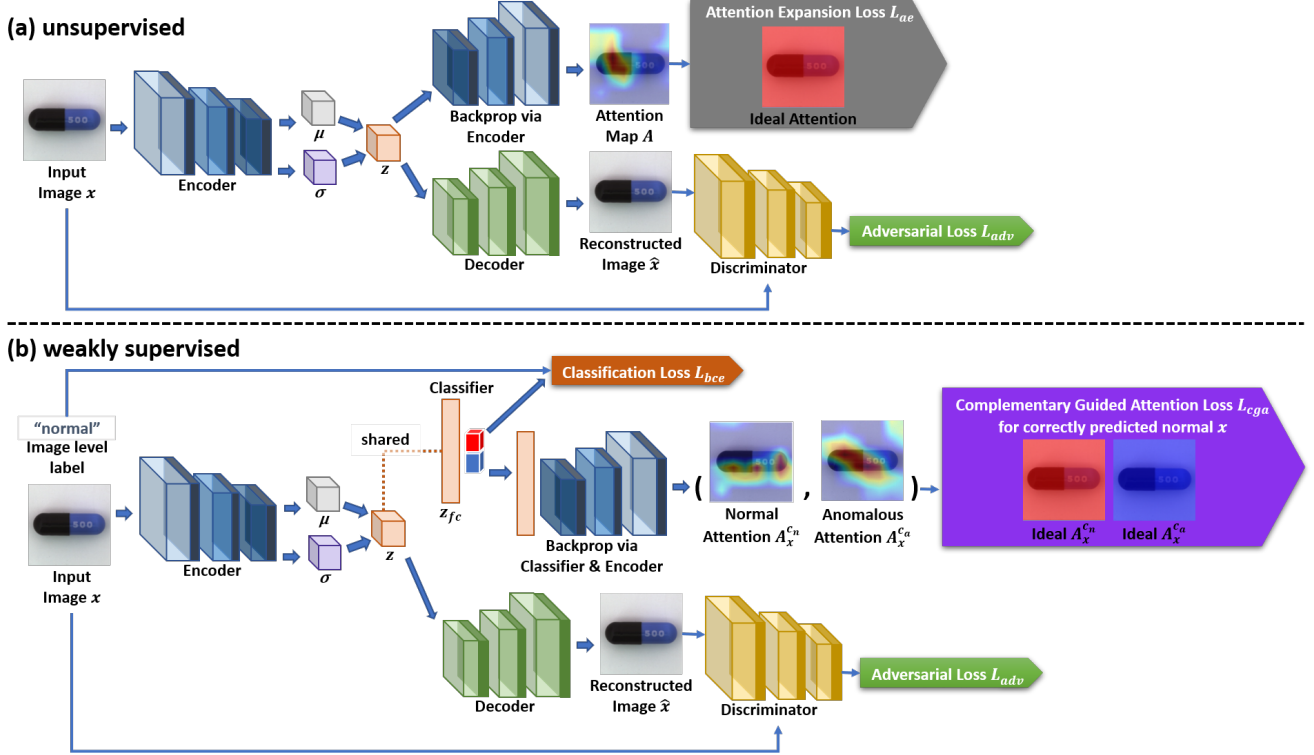
Figure 2. (a) The framework of CAVGA$_u$ where the attention expansion loss (L_{ae}) guides the attention map (A) computed from the latent variable z to cover the entire normal image. (b) The illustration of CAVGA$_w$ with the complementary guided attention loss (L_{cga}) to minimize the anomalous attention ($A_x^{c_a}$) and expand the normal attention $A_x^{c_n}$ for the normal images correctly predicted by the classifier.

2.1.2 Attention expansion loss L_{ae}

Along with detecting an image as anomalous, we also focus on spatially localizing the anomaly in the image. Most works [1, 33, 37] employ a thresholded pixel-wise difference between the reconstructed image and the input image to localize the anomaly where the threshold is determined by using anomalous training images. However, CAVGA$_u$ learns to localize the anomaly using an attention map reflected through an end-to-end training process without the need of any anomalous training images. We use the feature representation of the latent variable z to compute the attention map (A). A is computed using Grad-CAM [34] and normalized using a sigmoid operation such that $A_{i,j} \in [0, 1]$ to make it differentiable during the end-to-end training process.

Intuitively, A focuses on specific regions of the image based on the activation of neurons and its respective importance [40, 42]. Hence, it is required to focus on the entire image to localize the anomaly due to the lack of prior knowledge about the anomaly. We use this notion to learn the feature representation from the entire normal training image by proposing an attention expansion loss, where we encourage the network to generate an attention map that covers all the normal regions. This attention expansion loss

for each image $L_{ae,1}$ is formulated as follows:

$$L_{ae,1} = \frac{1}{|A|} \sum_{i,j} (1 - A_{i,j}) \qquad (3)$$

The final attention expansion loss L_{ae} is the average of $L_{ae,1}$ over the N images. We form the final objective function L_{final} below:

$$L_{final} = w_r L + w_{adv} L_{adv} + w_{ae} L_{ae}, \qquad (4)$$

where w_r, w_{adv}, and w_{ae} are the weights set as $1, 1$, and 0.01 respectively from validation.

During testing, we feed an image x_{test} into the encoder followed by the decoder, which reconstructs an image $\hat{x_{test}}$. As defined in [33], we compute the pixel-wise difference between $\hat{x_{test}}$ and x_{test} as the anomalous score s_a. Intuitively, if x_{test} is drawn from the learnt distribution of z, then s_a is small. Without using any anomalous training images in the unsupervised setting, we normalize s_a between $[0, 1]$ and empirically set 0.5 as the threshold to detect an image as anomalous. The attention map A_{test} is computed from z using Grad-CAM and is inverted ($\mathbf{1}$ - A_{test}) to obtain an anomalous attention map which localizes the anomaly. Here, $\mathbf{1}$ refers to a matrix of all ones with the same dimensions as A_{test}. We empirically choose 0.5

as the threshold on the anomalous attention map to evaluate the localization performance. We find that $CAVGA_u$ is insensitive to the threshold and outperforms the baselines with different threshold values.

2.2. Weakly supervised approach: $CAVGA_w$

$CAVGA_u$ can be further extended to a weakly supervised setting (denoted as $CAVGA_w$) where we explore the possibility of using few anomalous training images to improve the performance of anomaly detection and localization. Attention maps generated from a trained classifier have been used in weakly supervised semantic segmentation tasks [28, 34]. Given the labels of the anomalous and normal images without the pixel-wise annotation of the anomaly during training, we modify $CAVGA_u$ by introducing a binary classifier C at the output of z as shown in Figure 2 (b) and train C using the binary cross entropy loss L_{bce}. $CAVGA_w$ is jointly trained with L_{bce}, eq. 1, and eq. 2. Since the attention map depends on the performance of C [20], we propose the complementary guided attention loss based on C's prediction to better localize the anomaly.

Given an image x and its ground truth label y, we define $p \in \{c_a, c_n\}$ as the prediction of C, where c_a and c_n are the anomalous and normal classes respectively. From Figure 2 (b) we clone z into a new tensor, flatten it to form a fully connected layer z_{fc}, and add a 2-node output layer to form C. z and z_{fc} share parameters. For classification, we separately vectorize z_{fc}, which also enables the higher magnitude of gradient backpropagation from p [34].

We use Grad-CAM to compute the anomalous attention map $A_x^{c_a}$ for the anomalous class and the normal attention map $A_x^{c_n}$ for the normal class on the normal image x ($y = c_n$). Using the anomalous and normal attention maps, we propose a complementary guided attention loss where we minimize the areas covered by the anomalous attention map but simultaneously enforce the normal attention map to cover the entire normal image. Since the attention map is computed by backpropagating the gradients from p, any incorrect p would generate an undesired attention map. This would lead to the network learning to focus on erroneous areas of the image during training, which we avoid using the complementary guided attention loss. We compute this loss only for the normal images correctly classified by the classifier i.e. if $p = y = c_n$. We define $L_{cga,1}$, the complementary guided attention loss for each image, in the weakly supervised setting as:

$$L_{cga,1} = \frac{\mathbb{1}\,(p = y = c_n)}{|A_x^{c_n}|} \sum_{i,j}(1 - (A_x^{c_n})_{i,j} + (A_x^{c_a})_{i,j}), \quad (5)$$

where $\mathbb{1}\,(\cdot)$ is an indicator function. The final guided attention loss L_{cga} is the average of $L_{cga,1}$ over the N images.

property \ dataset	MVTAD [3]		mSTC [22]		D_M	D_F	D_C
setting	u	w	u	w	u	u	u
# classes/scenes	15/15	15/15	13/12	13/12	9/10	9/10	9/10
# n training images	3629	3629	244875	244875	∼59k	59k	45k
# a training images	0	35	0	1763	0	0	0
# n testing images	467	467	21147	21147	∼9k	9k	9k
# a testing images	1223	1223	86404	86404	∼1k	1k	1k

Table 1. Our experimental settings. The number of classes/scenes is in the form of training/testing. Notations: u: unsupervised; w: weakly supervised; n: normal; a: anomalous; D_M: MNIST [19]; D_F: Fashion-MNIST [39]; D_C: CIFAR-10 [17].

Our final objective function L_{final} is defined as:

$$L_{final} = w_r L + w_{adv}L_{adv} + w_c L_{bce} + w_{cga}L_{cga}, \quad (6)$$

where w_r, w_{adv}, w_c, and w_{cga} are weights set as $1, 1, 0.001$, and 0.01 respectively from validation. During testing, we use C to predict the input image x_{test} as anomalous or normal. The anomalous attention map A_{test} of x_{test} is computed when $y = c_a$. We use the same evaluation method as discussed in Sec. 2.1.2 for anomaly localization.

3. Experimental setup

Benchmark datasets: We evaluate CAVGA on the MVTAD [3], mSTC [22], MNIST [19], CIFAR-10 [17] and Fashion-MNIST [39] datasets for anomaly detection, and on the MVTAD and mSTC datasets for anomaly localization. Since the STC dataset [22] is designed for video instead of image anomaly detection, we extract every 5th frame of the video from each scene for training and testing without using any temporal information. We term the modified STC dataset as mSTC and summarize the experimental settings in Table 1.

Baseline methods: We compare $CAVGA_u$ and $CAVGA_w$ with AE_{L2} [4], AE_{SSIM} [4], AnoGAN [33], CNN feature dictionary (CNNFD) [27], texture inspection (TI) [5], and variation model (VM) [35] based approaches on the MVTAD and mSTC datasets. We also compare $CAVGA_u$ with CapsNet PP-based and CapsNet RE-based [21] (denoted as $CapsNet_{PP}$ and $CapsNet_{RE}$), AnoGAN [33], ADGAN [8], and β-VAE [14] on the MNIST, CIFAR-10 and Fashion-MNIST datasets.

Implementation details: All the images of the MVTAD and mSTC datasets are randomly center cropped to 256×256 and randomly rotated between $[-15°, +15°]$ to create variations in data during training. We train $CAVGA_u$ and $CAVGA_w$ with a learning rate of $1e^{-4}$ with a batch size of 16 for 150 epochs. To stabilize the training, the learning rate is decayed by $1e^{-1}$ for every 30 epochs. For the MNIST, CIFAR-10 and Fashion-MNIST datasets, we use the images of size 32×32 and follow the same data augmentation and training procedure as mentioned previously.

Architecture details: Based on the framework in Figure 2 (a), we use the convolution layers of ResNet-18 [13] as our encoder pretrained from the ImageNet [32] and fine-tune on each category / scenes individually. Inspired from [6], we propose to use the residual generator as our residual decoder by modifying it with a convolution layer interleaved between two upsampling (transpose convolution) layers to preserve local spatial information during reconstruction. The skip connection is added from the output of the upsampling layer to the output of the convolution layer to preserve the high-level feature information across upsampling layers. We use the discriminator of DC-GAN [30] pretrained on the Celeb-A dataset [24] and finetune on our data as our discriminator. This network is termed as CAVGA-R. For fair comparisons with the baseline approaches in terms of network architecture, we employ the discriminator and generator of DC-GAN pretrained on the Celeb-A dataset as our encoder and decoder respectively, and use the same discriminator as discussed previously to train this network (termed as CAVGA-D) using eq. 4 and eq. 6 and evaluate its performance for detection and localization. We refer to CAVGA-D_u and CAVGA-R_u as CAVGA$_u$ in the unsupervised setting, and CAVGA-D_w and CAVGA-R_w as CAVGA$_w$ in the weakly supervised setting respectively.

Training and evaluation: For anomaly detection on the MVTAD and mSTC datasets, the network is trained only on the normal images in the unsupervised setting. However, in the weakly supervised setting, since none of the baseline methods provide information on the number of anomalous training images they use to compute the threshold, we randomly choose 2% of the anomalous images along with all the normal training images for training. On the MNIST, CIFAR-10 and Fashion-MNIST datasets, we follow the same procedure as defined in [8] (i.e. in training and testing, we use a single class as anomalous and the rest of the classes as normal using which we train CAVGA-D_u.) Following [3], we use the mean of accuracy of correctly classified anomalous images and normal images to evaluate the performance of anomaly detection on both the normal and anomalous images on the MVTAD and mSTC datasets, while on the MNIST, CIFAR-10, and Fashion-MNIST datasets, same as [8], we use AuROC as our evaluation metric. For anomaly localization, we show the AuROC [3] and the Intersection-over-Union (IoU) between the generated attention map and the ground truth.

4. Experimental results

We use the cell color in the quantitative result tables to denote the performance ranking in that row, where darker cell color means better performance. Table 2 shows that CAVGA$_u$ localizes the anomaly better compared to the baselines in the unsupervised setting in IoU on the MVTAD
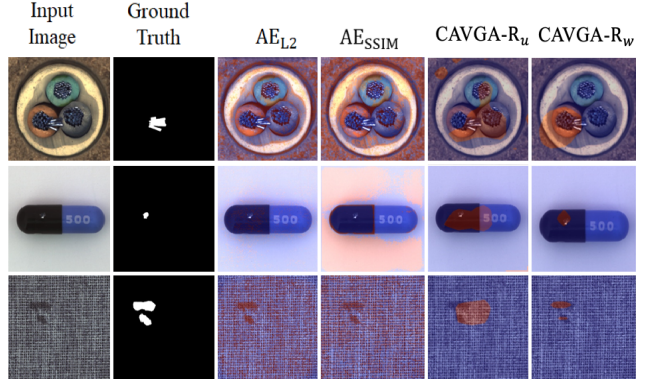

Figure 3. Qualitative results on the MVTAD dataset. The anomalous attention map (in red) depicts the localization of the anomaly.
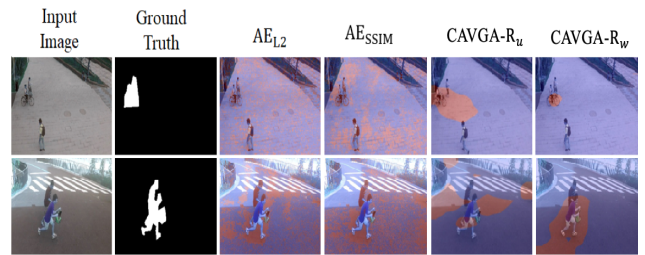

Figure 4. Qualitative results on the mSTC dataset.

dataset. Specifically, in 13 out of 15 categories, CAVGA-D_u outperforms the best performing baseline in these categories with an improvement ranging from 1% to 21% in IoU. CAVGA$_u$ also shows comparable results with the most competitive baseline AE$_{SSIM}$ in mean AuROC. Figure 3 shows the qualitative results on the MVTAD dataset. Table 3 shows that CAVGA$_u$ outperforms the baselines in the mean of accuracy of correctly classified anomalous images and normal images. CAVGA-D_u beats all the listed baselines in classification accuracy in 10 out of 15 categories with an improvement ranging from 1% to 26%. All baselines localize the anomaly from the thresholded pixelwise difference between the input and reconstructed image, where the threshold is computed using anomalous training images. *Needing no anomalous training images*, CAVGA-D_u still outperforms the methods that have access to anomalous training images. Table 2 shows that CAVGA-D_w localizes the anomaly better than CAVGA-D_u in all categories with an improvement ranging from 1% to 57%, and that CAVGA-D_w outperforms the best performing baseline in 13 out of 15 categories with an improvement between 1% and 45%. CAVGA$_w$ also outperforms the baselines in mean AuROC.

Table 2 and Table 3 show that AE$_{L2}$ and AE$_{SSIM}$ are the best performing methods for localization and classification accuracy as compared to other baselines, so we compare CAVGA with them on the mSTC dataset. Table 4 and Table 5 show that CAVGA also outperforms AE$_{L2}$

Category	AE_{SSIM} [4]	AE_{L2} [4]	AnoGAN [33]	CNNFD [27]	TI [5]	VM [35]	CAVGA-D_u	CAVGA-R_u	CAVGA-D_w	CAVGA-R_w
Bottle	0.15	0.22	0.05	0.07	-	0.03	0.30	0.34	0.36	0.39
Hazelnut	0.00	0.41	0.02	0.00	-	-	0.44	0.51	0.58	0.79
Capsule	0.09	0.11	0.04	0.00	-	0.01	0.25	0.31	0.38	0.41
Metal Nut	0.01	0.26	0.00	0.13	-	0.19	0.39	0.45	0.46	0.46
Leather	0.71	0.67	0.34	0.74	0.98	-	0.76	0.79	0.80	0.84
Pill	0.07	0.25	0.17	0.00	-	0.13	0.34	0.40	0.44	0.53
Wood	0.36	0.29	0.14	0.47	0.51	-	0.56	0.59	0.61	0.66
Carpet	0.69	0.38	0.34	0.20	0.29	-	0.71	0.73	0.70	0.81
Tile	0.04	0.23	0.08	0.14	0.11	-	0.31	0.38	0.68	0.81
Grid	0.88	0.83	0.04	0.02	0.01	-	0.32	0.38	0.42	0.55
Cable	0.01	0.05	0.01	0.13	-	-	0.37	0.44	0.49	0.51
Transistor	0.01	0.22	0.08	0.03	-	-	0.30	0.35	0.38	0.45
Toothbrush	0.08	0.51	0.07	0.00	-	0.24	0.54	0.57	0.60	0.63
Screw	0.03	0.34	0.01	0.00	-	0.12	0.42	0.48	0.51	0.66
Zipper	0.10	0.13	0.01	0.00	-	-	0.20	0.26	0.29	0.31
mean IoU	0.22	0.33	0.09	0.13	0.38	0.12	0.41	0.47	0.51	0.59
mean AuROC	0.87	0.82	0.74	0.78	0.76	0.77	0.85	0.89	0.92	0.93

Table 2. Performance comparison of anomaly localization in category specific IoU, mean IoU, and mean AuROC on the MVTAD dataset. The darker cell color indicates better performance ranking in each row.

Category	AE_{SSIM} [4]	AE_{L2} [4]	AnoGAN [33]	CNNFD [27]	TI [5]	VM [35]	CAVGA-D_u	CAVGA-R_u	CAVGA-D_w	CAVGA-R_w
Bottle	0.88	0.80	0.69	0.53	-	0.57	0.89	0.91	0.93	0.96
Hazelnut	0.54	0.88	0.50	0.49	-	-	0.84	0.87	0.90	0.92
Capsule	0.61	0.62	0.58	0.41	-	0.50	0.83	0.87	0.89	0.93
Metal Nut	0.54	0.73	0.50	0.65	-	0.58	0.67	0.71	0.81	0.88
Leather	0.46	0.44	0.52	0.67	0.50	-	0.71	0.75	0.80	0.84
Pill	0.60	0.62	0.62	0.46	-	0.57	0.88	0.91	0.93	0.97
Wood	0.83	0.74	0.68	0.84	0.71	-	0.85	0.88	0.89	0.89
Carpet	0.67	0.50	0.49	0.63	0.59	-	0.73	0.78	0.80	0.82
Tile	0.52	0.77	0.51	0.71	0.72	-	0.70	0.72	0.81	0.86
Grid	0.69	0.78	0.51	0.67	0.50	-	0.75	0.78	0.79	0.81
Cable	0.61	0.56	0.53	0.61	-	-	0.63	0.67	0.86	0.97
Transistor	0.52	0.71	0.67	0.58	-	-	0.73	0.75	0.80	0.89
Toothbrush	0.74	0.98	0.57	0.57	-	0.80	0.91	0.97	0.96	0.99
Screw	0.51	0.69	0.35	0.43	-	0.55	0.77	0.78	0.79	0.79
Zipper	0.80	0.80	0.59	0.54	-	-	0.87	0.94	0.95	0.96
mean	0.63	0.71	0.55	0.59	0.60	0.60	0.78	0.82	0.86	0.90

Table 3. The mean of accuracy of correctly classified anomalous images and normal images in anomaly detection on the MVTAD dataset.
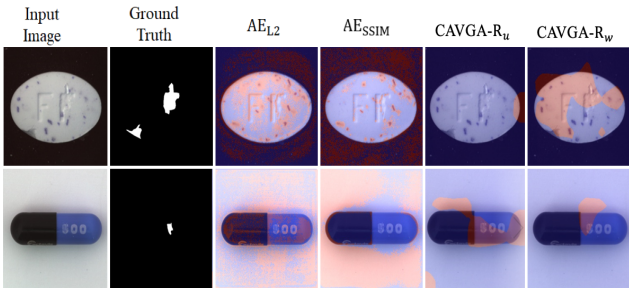

Figure 5. Examples of incorrect localization of the anomaly on the MVTAD dataset by CAVGA-R_u and CAVGA-R_w.

and AE_{SSIM} in IoU, AuROC, and classification accuracy on the mSTC dataset. Figure 4 shows the qualitative results on the mSTC dataset. Figure 5 illustrates that one challenge in anomaly localization is the potential low contrast between the anomalous regions and its background. In such scenarios, although still outperforming the baselines, CAVGA does not well localize the anomaly. Table 6 shows that CAVGA-D_u outperforms the most competitive baseline in AuROC in the unsupervised setting on the MNIST, CIFAR-10 and Fashion-MNIST datasets by 0.9%, 16.1%, and 15.7% respectively. Specifically, CAVGA-D_u outperforms the most competitive baseline in 6 out of 10 classes on the MNIST dataset and 7 out of 10 classes on the CIFAR-10 dataset. CAVGA-D_u also outperforms all the listed baselines in mean AuROC on the Fashion-MNIST dataset.

5. Ablation study

All the ablation studies are done on the MVTAD dataset where we illustrate the effectiveness of the convolutional z in CAVGA, L_{ae} in the unsupervised setting, and L_{cga} in the weakly supervised setting. The quantitative and qualitative results are shown in Table 7 and Figure 6 respectively.
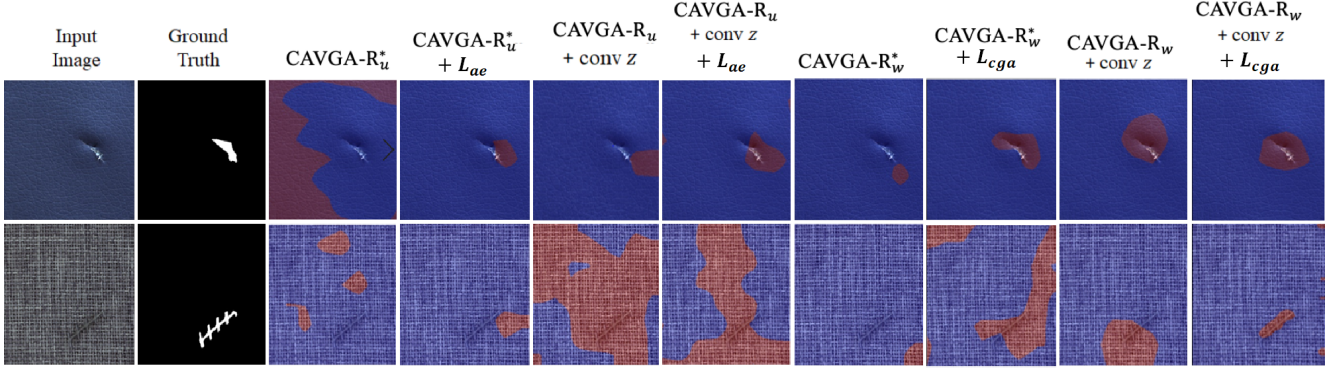
Figure 6. Qualitative results of the ablation study to illustrate the performance of the anomaly localization on the MVTAD dataset.

s_i	AE_{SSIM}	AE_{L2}	CAVGA-D_u	CAVGA-R_u	CAVGA-D_w	CAVGA-R_w
01	0.20	0.16	0.26	0.31	0.38	0.44
02	0.08	0.17	0.19	0.23	0.25	0.34
03	0.21	0.24	0.27	0.29	0.31	0.46
04	0.11	0.12	0.28	0.34	0.36	0.38
05	0.16	0.12	0.29	0.31	0.40	0.47
06	0.21	0.19	0.34	0.42	0.45	0.58
07	0.19	0.16	0.19	0.24	0.28	0.36
08	0.06	0.05	0.21	0.25	0.29	0.37
09	0.03	0.02	0.24	0.28	0.31	0.36
10	0.11	0.14	0.14	0.16	0.24	0.29
11	0.10	0.07	0.30	0.37	0.44	0.58
12	0.20	0.16	0.09	0.14	0.20	0.26
$\overline{IoU}$	0.14	0.13	0.23	0.28	0.33	0.41
$\overline{AuROC}$	0.76	0.74	0.83	0.85	0.89	0.90

Table 4. Performance comparison of anomaly localization in IoU on the mSTC dataset for each scene ID s_i and their mean ($\overline{IoU}$). We also list mean AuROC ($\overline{AuROC}$) here.

s_i	AE_{SSIM}	AE_{L2}	CAVGA-D_u	CAVGA-R_u	CAVGA-D_w	CAVGA-R_w
01	0.65	0.72	0.77	0.85	0.84	0.87
02	0.70	0.61	0.76	0.84	0.89	0.90
03	0.79	0.71	0.82	0.84	0.86	0.88
04	0.81	0.66	0.80	0.80	0.81	0.83
05	0.71	0.67	0.81	0.86	0.90	0.94
06	0.47	0.55	0.64	0.67	0.65	0.70
07	0.36	0.59	0.60	0.64	0.75	0.77
08	0.69	0.70	0.74	0.74	0.76	0.80
09	0.84	0.73	0.87	0.88	0.90	0.91
10	0.83	0.88	0.88	0.92	0.94	0.94
11	0.71	0.75	0.79	0.81	0.83	0.83
12	0.65	0.52	0.76	0.79	0.81	0.83
avg	0.68	0.67	0.77	0.80	0.83	0.85

Table 5. Anomaly detection performance in the mean of accuracy of correctly classified anomalous images and normal images on the mSTC dataset for each scene ID s_i and their mean (avg).

Effect of convolutional latent variable z: To show the effectiveness of the convolutional z, we flatten the output of the encoder of CAVGA-R_u and CAVGA-R_w, and connect it to a fully connected layer as latent variable with dimen-

sion 100. The dimension of the latent variable is chosen from validation. We call these network as CAVGA-R_u^* and CAVGA-R_w^* in the unsupervised and weakly supervised settings respectively. In the unsupervised setting, we train CAVGA-R_u and CAVGA-R_u^* individually using $L + L_{adv}$ as our objective function and compute the anomalous attention map from the feature map of the latent variable during inference. Similarly, in the weakly supervised setting, we train CAVGA-R_w and CAVGA-R_w^* individually using $L + L_{adv} + L_{bce}$ as our objective function and compute the anomalous attention map from the classifier's prediction during inference. Comparing Column ID 1 with 3 and 5 with 7 in Table 7, we observe that preserving the spatial relation of the input and latent variable through the convolutional z improves the IoU in anomaly localization without the use of L_{ae} in the unsupervised setting and L_{cga} in the weakly supervised setting. Furthermore, comparing Column ID 2 with 4 and 6 with 8 in Table 7, we observe that using convolutional z in CAVGA-R_u and CAVGA-R_w outperforms using a flattened latent variable even with the help of L_{ae} in the unsupervised setting and L_{cga} in the weakly supervised setting.

Effect of attention expansion loss L_{ae}: To test the effectiveness of using L_{ae} in the unsupervised setting, we train CAVGA-R_u^* and CAVGA-R_u with eq. 4 included in the objective function. During inference, the anomalous attention map is computed to localize the anomaly. Comparing Column ID 1 with 2 and 3 with 4 in Table 7, we observe that L_{ae} enhances the IoU regardless of whether the latent variable is flattened or convolutional.

Effect of complementary guided attention loss L_{cga}: We show the effectiveness of L_{cga} by including it in the objective function of CAVGA-R_w^* and CAVGA-R_w. Comparing Column ID 5 with 6 and 7 with 8 in Table 7, we find that using L_{cga} enhances the IoU regardless of whether the latent variable is flattened or convolutional.

Dataset	Class	CapsNet$_{PP}$ [21]	CapsNet$_{RE}$ [21]	AnoGAN [33]	ADGAN [8]	β-VAE [14]	CAVGA-D$_u$
MNIST [19]	0	0.998	0.947	0.990	0.999	0.890	0.994
	1	0.990	0.907	0.998	0.992	0.841	0.997
	2	0.984	0.970	0.888	0.968	0.967	0.989
	3	0.976	0.949	0.913	0.953	0.947	0.983
	4	0.935	0.872	0.944	0.960	0.968	0.977
	5	0.970	0.966	0.912	0.955	0.966	0.968
	6	0.942	0.909	0.925	0.980	0.907	0.988
	7	0.987	0.934	0.964	0.950	0.899	0.986
	8	0.993	0.929	0.883	0.959	0.946	0.988
	9	0.990	0.871	0.958	0.965	0.794	0.991
	mean	0.977	0.925	0.937	0.968	0.913	0.986
CIFAR-10 [17]	0	0.622	0.371	0.610	0.661	0.368	0.653
	1	0.455	0.737	0.565	0.435	0.746	0.784
	2	0.671	0.421	0.648	0.636	0.397	0.761
	3	0.675	0.588	0.528	0.488	0.604	0.747
	4	0.683	0.388	0.670	0.794	0.387	0.775
	5	0.635	0.601	0.592	0.640	0.611	0.552
	6	0.727	0.491	0.625	0.685	0.500	0.813
	7	0.673	0.631	0.576	0.559	0.614	0.745
	8	0.710	0.410	0.723	0.798	0.399	0.801
	9	0.466	0.671	0.582	0.643	0.698	0.730
	mean	0.612	0.531	0.612	0.634	0.532	0.736
Fashion MNIST [39]	mean	0.765	0.679	-	-	0.683	0.885

Table 6. Performance comparison in terms of AuROC and mean AuROC with the state-of-the-art methods on the MNIST and CIFAR-10 datasets. We also report the mean AuROC on the Fashion-MNIST dataset here.

Category	CAVGA-R$_u^*$	CAVGA-R$_u^*$ $+ L_{ae}$	CAVGA-R$_u$ $+$ conv z	CAVGA-R$_u$ $+$ conv $z + L_{ae}$	CAVGA-R$_w^*$	CAVGA-R$_w^*$ $+ L_{cga}$	CAVGA-R$_w$ $+$ conv z	CAVGA-R$_w$ $+$ conv $z+ L_{cga}$
Column ID	1	2	3	4	5	6	7	8
Bottle	0.24	0.27	0.26	0.33	0.16	0.34	0.28	0.39
Hazelnut	0.16	0.26	0.31	0.47	0.51	0.76	0.67	0.79
Capsule	0.09	0.22	0.14	0.31	0.18	0.36	0.27	0.41
Metal Nut	0.28	0.38	0.34	0.45	0.25	0.38	0.28	0.46
Leather	0.55	0.71	0.64	0.79	0.72	0.79	0.75	0.84
Pill	0.24	0.35	0.29	0.40	0.24	0.44	0.43	0.53
Wood	0.25	0.43	0.36	0.59	0.51	0.62	0.61	0.66
Carpet	0.48	0.59	0.53	0.73	0.69	0.78	0.72	0.81
Tile	0.07	0.18	0.23	0.32	0.66	0.77	0.73	0.81
Grid	0.15	0.27	0.24	0.32	0.31	0.48	0.51	0.55
Cable	0.30	0.38	0.36	0.43	0.47	0.58	0.51	0.63
Transistor	0.17	0.29	0.26	0.34	0.33	0.41	0.39	0.45
Toothbrush	0.41	0.46	0.49	0.55	0.54	0.61	0.60	0.66
Screw	0.11	0.18	0.34	0.48	0.16	0.24	0.22	0.31
Zipper	0.07	0.18	0.21	0.25	0.19	0.24	0.29	0.31
mean	0.24	0.34	0.33	0.47	0.39	0.52	0.48	0.60

Table 7. The ablation study showing the IoU in anomaly localization on the MVTAD dataset. CAVGA-R$_u^*$ and CAVGA-R$_w^*$ are our base architecture with a flattened z in the unsupervised and weakly supervised settings respectively. "conv z" means using convolutional z.

6. Conclusion

We propose the first end-to-end trainable convolutional adversarial variational autoencoder using guided attention (CAVGA) to address anomaly detection and localization with attention maps. Applicable to different network architectures, our attention expansion loss and complementary guided attention loss improve the performance of anomaly detection and localization in the unsupervised and weakly supervised (with only 2% extra anomalous images for training) settings respectively. We quantitatively and qualitatively show that CAVGA outperforms the state-of-the-art (SOTA) anomaly detection methods in the unsupervised setting on the MNIST, Fashion-MNIST, CIFAR-10, MVTec Anomaly Detection (MVTAD), and modified ShanghaiTech Campus (mSTC) datasets. CAVGA also outperforms the SOTA anomaly localization methods in the weakly supervised setting on the MVTAD and mSTC datasets.

References

[1] Samet Akcay, Amir Atapour-Abarghouei, and Toby P Breckon. GANomaly: Semi-supervised anomaly detection via adversarial training. In *Asian Conference on Computer Vision*, pages 622–637. Springer, 2018.

[2] Yannick Benezeth, P-M Jodoin, Venkatesh Saligrama, and Christophe Rosenberger. Abnormal events detection based on spatio-temporal co-occurences. In *2009 IEEE Conference on Computer Vision and Pattern Recognition*, pages 2458–2465. IEEE, 2009.

[3] Paul Bergmann, Michael Fauser, David Sattlegger, and Carsten Steger. MVTec AD–a comprehensive real-world dataset for unsupervised anomaly detection. In *Proceedings of the IEEE Conference on Computer Vision and Pattern Recognition*, pages 9592–9600, 2019.

[4] Paul Bergmann, Sindy Löwe, Michael Fauser, David Sattlegger, and Carsten Steger. Improving unsupervised defect segmentation by applying structural similarity to autoencoders. In *International Joint Conference on Computer Vision, Imaging and Computer Graphics Theory and Applications (VISIGRAPP)*, volume 5, 2019.

[5] Tobias Böttger and Markus Ulrich. Real-time texture error detection on textured surfaces with compressed sensing. *Pattern Recognition and Image Analysis*, 26(1):88–94, 2016.

[6] Andrew Brock, Jeff Donahue, and Karen Simonyan. Large scale GAN training for high fidelity natural image synthesis. In *International Conference on Learning Representations*, 2019.

[7] Kai-Wen Cheng, Yie-Tarng Chen, and Wen-Hsien Fang. Abnormal crowd behavior detection and localization using maximum sub-sequence search. In *Proceedings of the 4th ACM/IEEE international workshop on Analysis and retrieval of tracked events and motion in imagery stream*, pages 49–58. ACM, 2013.

[8] Lucas Deecke, Robert Vandermeulen, Lukas Ruff, Stephan Mandt, and Marius Kloft. Image anomaly detection with generative adversarial networks. In *Joint European Conference on Machine Learning and Knowledge Discovery in Databases*, pages 3–17. Springer, 2018.

[9] Asimenia Dimokranitou. *Adversarial autoencoders for anomalous event detection in images*. PhD thesis, 2017.

[10] Rohit Girdhar, Joao Carreira, Carl Doersch, and Andrew Zisserman. Video action transformer network. In *Proceedings of the IEEE Conference on Computer Vision and Pattern Recognition*, pages 244–253, 2019.

[11] Matheus Gutoski, Nelson Marcelo Romero Aquino, Manassés Ribeiro, EA Lazzaretti, and SH Lopes. Detection of video anomalies using convolutional autoencoders and one-class support vector machines. In *XIII Brazilian Congress on Computational Intelligence, 2017*, 2017.

[12] Mahmudul Hasan, Jonghyun Choi, Jan Neumann, Amit K Roy-Chowdhury, and Larry S Davis. Learning temporal regularity in video sequences. In *Proceedings of the IEEE Conference on Computer Vision and Pattern Recognition*, pages 733–742, 2016.

[13] Kaiming He, Xiangyu Zhang, Shaoqing Ren, and Jian Sun. Deep residual learning for image recognition. In *Proceedings of the IEEE Conference on Computer Vision and Pattern Recognition*, pages 770–778, 2016.

[14] Irina Higgins, Loic Matthey, Arka Pal, Christopher Burgess, Xavier Glorot, Matthew Botvinick, Shakir Mohamed, and Alexander Lerchner. beta-VAE: Learning basic visual concepts with a constrained variational framework. *International Conference on Learning Representations*, 2(5):6, 2017.

[15] Diederik P. Kingma and Max Welling. Auto-encoding variational bayes. In *International Conference on Learning Representations*, 2014.

[16] B Kiran, Dilip Thomas, and Ranjith Parakkal. An overview of deep learning based methods for unsupervised and semi-supervised anomaly detection in videos. *Journal of Imaging*, 4(2):36, 2018.

[17] Alex Krizhevsky, Geoffrey Hinton, et al. Learning multiple layers of features from tiny images. Technical report, Citeseer, 2009.

[18] Anders Boesen Lindbo Larsen, Søren Kaae Sønderby, Hugo Larochelle, and Ole Winther. Autoencoding beyond pixels using a learned similarity metric. In *International Conference on Machine Learning*, 2016.

[19] Yann LeCun, Léon Bottou, Yoshua Bengio, Patrick Haffner, et al. Gradient-based learning applied to document recognition. *Proceedings of the IEEE*, 86(11):2278–2324, 1998.

[20] Kunpeng Li, Ziyan Wu, Kuan-Chuan Peng, Jan Ernst, and Yun Fu. Tell me where to look: Guided attention inference network. In *Proceedings of the IEEE Conference on Computer Vision and Pattern Recognition*, pages 9215–9223, 2018.

[21] Xiaoyan Li, Iluju Kiringa, Tet Yeap, Xiaodan Zhu, and Yifeng Li. Exploring deep anomaly detection methods based on capsule net. *International Conference on Machine Learning 2019 Workshop on Uncertainty and Robustness in Deep Learning*, 2019.

[22] Wen Liu, Weixin Luo, Dongze Lian, and Shenghua Gao. Future frame prediction for anomaly detection–a new baseline. In *Proceedings of the IEEE Conference on Computer Vision and Pattern Recognition*, pages 6536–6545, 2018.

[23] Weiyang Liu, Yandong Wen, Zhiding Yu, Ming Li, Bhiksha Raj, and Le Song. Sphereface: Deep hypersphere embedding for face recognition. In *Proceedings of the IEEE Conference on Computer Vision and Pattern Recognition*, pages 212–220, 2017.

[24] Ziwei Liu, Ping Luo, Xiaogang Wang, and Xiaoou Tang. Deep learning face attributes in the wild. In *Proceedings of International Conference on Computer Vision (ICCV)*, December 2015.

[25] Alireza Makhzani, Jonathon Shlens, Navdeep Jaitly, Ian Goodfellow, and Brendan Frey. Adversarial autoencoders. In *International Conference on Learning Representations*, 2016.

[26] Andriy Myronenko. 3D MRI brain tumor segmentation using autoencoder regularization. In *International MICCAI Brainlesion Workshop*, pages 311–320. Springer, 2018.

[27] Paolo Napoletano, Flavio Piccoli, and Raimondo Schettini. Anomaly detection in nanofibrous materials by CNN-based self-similarity. *Sensors*, 18(1):209, 2018.

[28] Maxime Oquab, Léon Bottou, Ivan Laptev, and Josef Sivic.

Is object localization for free?-weakly-supervised learning with convolutional neural networks. In *Proceedings of the IEEE Conference on Computer Vision and Pattern Recognition*, pages 685–694, 2015.

[29] Nick Pawlowski, Matthew CH Lee, Martin Rajchl, Steven McDonagh, Enzo Ferrante, Konstantinos Kamnitsas, Sam Cooke, Susan Stevenson, Aneesh Khetani, Tom Newman, et al. Unsupervised lesion detection in brain CT using bayesian convolutional autoencoders. In *Medical Imaging with Deep Learning*, 2018.

[30] Alec Radford, Luke Metz, and Soumith Chintala. Unsupervised representation learning with deep convolutional generative adversarial networks. In *International Conference on Learning Representations*, 2016.

[31] Mahdyar Ravanbakhsh, Enver Sangineto, Moin Nabi, and Nicu Sebe. Training adversarial discriminators for cross-channel abnormal event detection in crowds. In *2019 IEEE Winter Conference on Applications of Computer Vision (WACV)*, pages 1896–1904. IEEE, 2019.

[32] Olga Russakovsky, Jia Deng, Hao Su, Jonathan Krause, Sanjeev Satheesh, Sean Ma, Zhiheng Huang, Andrej Karpathy, Aditya Khosla, Michael Bernstein, et al. ImageNet large scale visual recognition challenge. *International journal of computer vision*, 115(3):211–252, 2015.

[33] Thomas Schlegl, Philipp Seeböck, Sebastian M Waldstein, Ursula Schmidt-Erfurth, and Georg Langs. Unsupervised anomaly detection with generative adversarial networks to guide marker discovery. In *International Conference on Information Processing in Medical Imaging*, pages 146–157. Springer, 2017.

[34] Ramprasaath R Selvaraju, Michael Cogswell, Abhishek Das, Ramakrishna Vedantam, Devi Parikh, and Dhruv Batra. Grad-cam: Visual explanations from deep networks via gradient-based localization. In *Proceedings of the IEEE International Conference on Computer Vision*, pages 618–626, 2017.

[35] Carsten Steger. Similarity measures for occlusion, clutter, and illumination invariant object recognition. In *Joint Pattern Recognition Symposium*, pages 148–154. Springer, 2001.

[36] Du Tran and Junsong Yuan. Optimal spatio-temporal path discovery for video event detection. In *Proceedings of the IEEE Conference on Computer Vision and Pattern Recognition*, pages 3321–3328. IEEE, 2011.

[37] Ha Son Vu, Daisuke Ueta, Kiyoshi Hashimoto, Kazuki Maeno, Sugiri Pranata, and Sheng Mei Shen. Anomaly detection with adversarial dual autoencoders. *arXiv preprint arXiv:1902.06924*, 2019.

[38] Siqi Wang, En Zhu, Jianping Yin, and Fatih Porikli. Video anomaly detection and localization by local motion based joint video representation and ocelm. *Neurocomputing*, 277:161–175, 2018.

[39] Han Xiao, Kashif Rasul, and Roland Vollgraf. Fashion-MNIST: a novel image dataset for benchmarking machine learning algorithms. *arXiv preprint arXiv:1708.07747*, 2017.

[40] Sergey Zagoruyko and Nikos Komodakis. Paying more attention to attention: Improving the performance of convolutional neural networks via attention transfer. In *International Conference on Learning Representations*, 2017.

[41] Houssam Zenati, Chuan Sheng Foo, Bruno Lecouat, Gaurav Manek, and Vijay Ramaseshan Chandrasekhar. Efficient GAN-based anomaly detection. *arXiv preprint arXiv:1802.06222*, 2018.

[42] Bolei Zhou, Aditya Khosla, Agata Lapedriza, Aude Oliva, and Antonio Torralba. Learning deep features for discriminative localization. In *Proceedings of the IEEE conference on computer vision and pattern recognition*, pages 2921–2929, 2016.